

Superconductivity at 3.5 K and/or 7.2 K in potassium-doped triphenylbismuth

Ren-Shu Wang, Jia Cheng, Xiao-Lin Wu, Hui Yang, Xiao-Jia Chen, Yun Gao, and Zhong-Bing Huang

Citation: *The Journal of Chemical Physics* **149**, 144502 (2018); doi: 10.1063/1.5045631

View online: <https://doi.org/10.1063/1.5045631>

View Table of Contents: <http://aip.scitation.org/toc/jcp/149/14>

Published by the *American Institute of Physics*

PHYSICS TODAY

WHITEPAPERS

ADVANCED LIGHT CURE ADHESIVES

Take a closer look at what these environmentally friendly adhesive systems can do

READ NOW

PRESENTED BY
MASTERBOND
ADHESIVES | SEALANTS | COATINGS

Superconductivity at 3.5 K and/or 7.2 K in potassium-doped triphenylbismuth

Ren-Shu Wang,^{1,2} Jia Cheng,¹ Xiao-Lin Wu,¹ Hui Yang,¹ Xiao-Jia Chen,^{2,a)} Yun Gao,^{1,b)} and Zhong-Bing Huang^{1,c)}

¹*School of Materials Science and Engineering, Faculty of Physics and Electronic Technology, Hubei University, Wuhan 430062, China*

²*Center for High Pressure Science and Technology Advanced Research, Shanghai 201203, China*

HPSTAR
631-2018

(Received 22 June 2018; accepted 20 September 2018; published online 11 October 2018)

We develop a two-step synthesis method—ultrasound treatment and low temperature annealing to explore superconductivity in potassium-doped triphenylbismuth, which is composed of one bismuth atom and three phenyl rings. The combination of dc and ac magnetic measurements reveals that one hundred percent of synthesized samples exhibit superconductivity at 3.5 K and/or 7.2 K at ambient pressure. The magnetization hysteresis loops provide a strong piece of evidence of type-II superconductors. It is found that the doped materials crystallize into the triclinic P1 structure, with a mole ratio of 4:1 between potassium and triphenylbismuth. Both the calculated electronic structure and measured Raman spectra indicate that superconductivity is realized by transferring electrons from the K-4s to C-2p orbital. Our study opens an encouraging window for the search of organic superconductors in organometallic molecules. *Published by AIP Publishing.* <https://doi.org/10.1063/1.5045631>

I. INTRODUCTION

Superconductivity in organic materials has been attracting great attention due to its fundamental importance and potential application prospect. Similar to well-known iron-based and cuprate high temperature superconductors, organic superconductors provide ideal model systems for understanding the interplay of electron-electron and electron-lattice interactions, as well as the proximity of magnetism and unconventional superconductivity in reduced dimensions. Following the discovery of superconductivity in (TMTSF)₂PF₆ in 1980,¹ several organic superconducting (SC) families have been reported including charge transfer complexes,^{2,3} fullerides,⁴⁻⁶ graphites,⁷⁻¹⁰ and graphene superlattices.^{11,12} Among them, fullerides hold the record for an SC transition temperature T_c of 38 K.⁵

In 2010, potassium-doped picene was shown to display a SC transition temperature T_c as high as 18 K,¹³ which provides a platform to explore superconductivity in organic hydrocarbons. Soon thereafter, potassium-doped phenanthrene¹⁴ and dibenzopentacene¹⁵ were found to exhibit superconductivity at 5 K and 33 K, respectively. The above three molecules belong to fused hydrocarbons, in which five, three, and seven phenyl rings are fused via sharing sides. Very recently, we found that by doping potassium into *p*-terphenyl, a hydrocarbon formed by connecting three phenyl rings with the C-C bond, SC transitions can be observed at 123 K, 43 K, and 7.2 K.¹⁶ Superconductivity-like transitions above 100 K were also observed in potassium-doped *p*-terphenyl by other

research groups.^{17,18} Meanwhile, an energy gap persisting up to 120 K in potassium surface-doped *p*-terphenyl crystals from photoemission spectroscopy provides a strong piece of evidence for the formation of Cooper pairs that is a prerequisite for high temperature superconductivity.¹⁹

Despite tremendous efforts by the scientific community,²⁰⁻³⁷ the detailed crystal structures of hydrocarbon superconductors have not yet been determined in experiments so far, due to low reproducibility of SC samples and vanishingly small SC fractions. This places a serious restriction on the deep understanding of their physical properties. To make progress on hydrocarbon superconductors, we develop a two-step synthesis method—ultrasound treatment and low temperature annealing to explore superconductivity in potassium-doped triphenylbismuth. As a member of organometallic molecules,³⁸ triphenylbismuth has been used as the solidifying catalyst for butyl hydroxyl propellants of high combustion velocity, as well as the catalyst for some monomers' polymerization.³⁹ In each triphenylbismuth molecule, three phenyl rings and one bismuth atom are connected by a single C-Bi bond. Such an arrangement of phenyl rings is distinct from the ones in fullerides,^{4,5} graphites,^{7,8} fused hydrocarbons,¹³⁻¹⁵ and *p*-terphenyl.¹⁶ In view of these facts, exploration of superconductivity in potassium-doped triphenylbismuth not only enriches the functionalities of organometallic compounds but also provides a new platform for understanding the relationship between the SC property and molecular structure.

The paper is organized as follows. In Sec. II, we describe the synthesis and characterization of potassium-doped triphenylbismuth and present the details of theoretical calculations. In Sec. III, the results obtained are described and discussed. In Sec. IV, the conclusions are presented.

^{a)}Electronic mail: xjchen@hpstar.ac.cn

^{b)}Electronic mail: gaoyun@hubeu.edu.cn

^{c)}Electronic mail: huangzb@hubeu.edu.cn

II. EXPERIMENTS AND THEORETICAL CALCULATIONS

A. Material synthesis

High-purity potassium metal (99% purity, Sinopharm Chemical Reagent) was cut into small pieces and mixed with triphenylbismuth (>98% purity, Tokyo Chemical Industry) with a nominal mole ratio of x : 1 ($x = 1, 2, 2.5, 3, \text{ and } 3.5$). Each mixture with a fixed x was then loaded into a quartz tube and sealed under a vacuum about (1×10^{-4} Pa). The sample tubes were treated in an ultrasound device at 90°C for 10 h. After ultrasound treatment, the samples tubes were heated at 130°C for 1-5 days. Here, the ultrasound treatment was adopted to mix potassium and triphenylbismuth thoroughly, and low temperature annealing can avoid producing KH via reaction of potassium and hydrogen, which is crucial for crystallization of doped materials.

B. Material characterization

For each run of experiment, the sample from the same tube was distributed into several nonmagnetic capsules and sealed by GE varnish in a glove box with the oxygen and moisture levels less than 0.1 ppm. Magnetization measurements were performed with a SQUID magnetometer (Quantum Design MPMS3) in the temperature range of 1.8–300 K. The crystal structures of pristine and potassium-doped materials were measured on an X-ray diffraction (XRD) spectrometer (Panalytical Emperean). The Raman scattering spectra were collected at room temperature on an in-house system with a charge coupled device and spectrometer from Princeton Instruments in a wavelength of 660 nm and power less than 1 mW.

C. Theoretical calculations

The Universal Structure Predictor: Evolutionary Xtallography (USPEX)⁴⁰ based on the genetic algorithm has been employed to search for global stable or metastable structures in the phase diagram of K_xBi with $y = 1-4$ at a temperature of 0 K and a pressure of 0 GPa. In the search process, the plane-wave pseudopotential method as implemented in the Vienna *ab initio* simulation package (VASP) program^{41,42} was adopted to relax

the atomic positions. The generalized gradient approximation (GGA) with the Perdew-Burke-Ernzerhof (PBE) formula⁴³ for the exchange-correlation potentials and the projector-augmented wave (PAW) method⁴⁴ for ionic potentials were used to model the electron-electron and electron-ion interactions. Plane wave basis sets with an energy cutoff of 450 eV and $3 \times 3 \times 3$ Monkhorst-Pack k-points mesh were adopted for geometry optimization. A finer $5 \times 5 \times 5$ k-point sampling scheme was used for calculating the partial density of states (PDOS). The convergence criteria for the energy and maximum force are set to 10^{-4} eV and 0.01 eV/Å, respectively.

III. RESULTS AND DISCUSSIONS

A. Magnetic property of potassium-doped triphenylbismuth

Pristine triphenylbismuth exhibits a weak diamagnetic behavior, which is clearly characterized by the small negative magnetic susceptibility in the temperature range of 1.8–300 K. Upon doping potassium into triphenylbismuth, all synthesized samples listed in Table I exhibit a SC transition temperature of ~ 3.5 K, and four samples also show a transition at 7.2 K. The observation of similar SC transitions in the samples with different x 's between potassium and triphenylbismuth indicates that the actual mole ratio is independent of the nominal value. The last column in Table I shows the superconducting fraction (SF) of the common 3.5 K superconducting phase, estimated from the magnetic susceptibility at 1.8 K. All samples except sample D have SFs less than 1%. The small SFs indicate that the observed superconductivity is granular or filamentary, not bulk. The reasons for the small SFs will be given in Subsection III B.

The representative results for samples D ($x = 3$, annealed for 3 days) and E ($x = 2$, annealed for 5 days) are summarized in Fig. 1. Figure 1(a) shows the dc magnetic susceptibility χ for sample D in the applied magnetic field of 10 Oe with field cooling (FC) and zero-field cooling (ZFC) in the temperature range of 1.8–11 K. Both FC and ZFC susceptibilities show a sudden decrease around 3.5 K. Such a sudden drop of χ is consistent with the well-defined Meissner effect,

TABLE I. List of K_x triphenylbismuth samples synthesized in this study. Both T_c^{onset} and T_c indicated by two black arrows in Fig. 1(a) were read out from the ZFC run measured in the applied magnetic field of 10 Oe. The former denotes the temperature where the magnetic susceptibility turns to suddenly decrease with lowering the temperature, and the latter is determined from the intercept of linear extrapolations from below and above T_c^{onset} . The linear extrapolations are represented by two gray lines in Fig. 1(a). The SFs for the 3.5 K SC phase of different samples are shown in the last column. The boldface values highlight the representative samples D and E.

Sample label	x	Annealing time (days)	T_c^{onset}	T_c	SF(1.8 K) (%)
A	3	1	3.39	3.19	0.26
B	1	3	3.06	2.90	0.01
C	2	3	3.56 and 7.28	3.35 and 7.19	0.44
D	3	3	3.49	3.32	3.74
E	2	5	3.51 and 7.18	3.29 and 7.13	0.12
F	2.5	5	3.46	3.30	0.11
G	3	5	3.52 and 7.17	3.32 and 7.06	0.02
H	3.5	5	3.53 and 7.25	3.28 and 7.13	0.02

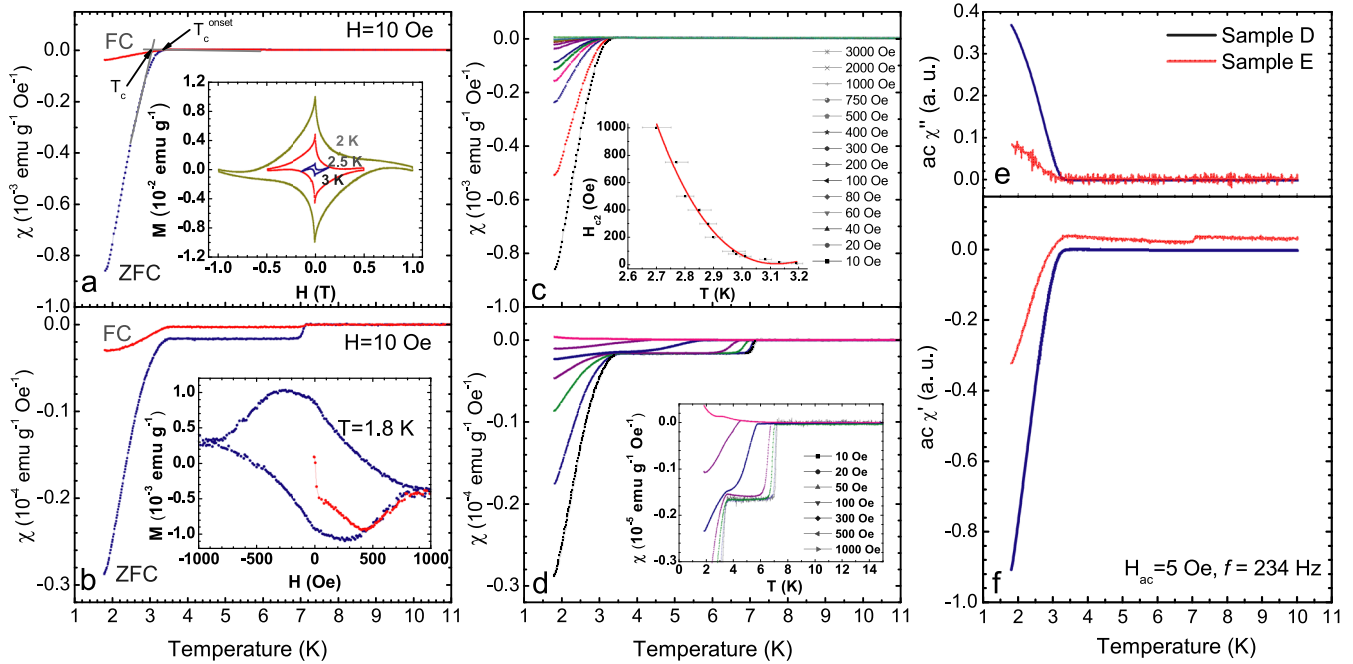


FIG. 1. [(a) and (b)] The temperature dependence of the dc magnetic susceptibility χ for samples D and E in the applied magnetic field of 10 Oe with field cooling (FC) and zero-field cooling (ZFC). The inset figures show the magnetization loops of samples D and E, with the measured temperature shown beside the corresponding loop. [(c) and (d)] The temperature dependence of χ for samples D and E measured at various magnetic fields in the ZFC run. The inset figure in (c) shows the upper critical magnetic field H_{c2} in the temperature region of 2.7–3.2 K. The inset figure in (d) displays the transition around 7.2 K with enlarged scale. [(e) and (f)] Imaginary χ'' and real χ' components of the ac magnetic susceptibility as a function of temperature. The probe harmonic magnetic field and frequency are 5 Oe and 234 Hz, respectively.

supporting the occurrence of superconductivity in sample D. Similarly, sudden drops of χ around 3.5 and 7.2 K indicate that there exist two SC phases in sample E [Fig. 1(b)]. Notice that the drop at 7.2 K is much weaker than the one at 3.5 K, implying that sample E is dominated by the SC phase with $T_c \sim 3.5$ K.

The inset of Fig. 1(a) shows the magnetization loops of sample D with the magnetic field up to 1.0 T measured at 2, 2.5, and 3 K in the SC state. The hysteresis loops along the two opposite magnetic field directions show a clear diamond-like shape, providing a strong piece of evidence for the type-II superconductor. One can readily see that the dip or peak of the magnetization loops appears at a magnetic field close to 0 T, indicating a very small lower critical magnetic field H_{c1} for the SC phase at 3.5 K. The expansion of the diamond from 3 K to 2 K reflects the fact that the upper critical magnetic field H_{c2} increases with lowering temperature. The type-II SC behavior is also applied for sample E, as seen from the magnetization loop with a magnetic field up to 1000 Oe measured at 1.8 K in the inset of Fig. 1(b). One significant difference from the magnetization loops of sample D is that the diamond shape is strongly distorted due to the coexistence of two SC phases in sample E.

The obtained superconductivity in potassium-doped triphenylbismuth was also supported by the evolution of the χ -T curve with the applied magnetic fields [Figs. 1(c) and 1(d) and the inset of Fig. 1(d)]. The χ -T curve gradually shifts toward the lower temperatures with increasing magnetic field. This character is consistent with the intrinsic property of a superconductor; i.e., the SC transition temperature T_c is gradually decreased with increasing magnetic field. In the inset

of Fig. 1(c), we show the temperature dependence of the upper critical magnetic field H_{c2} for sample D in the temperature region of 2.7–3.2 K. Here, H_{c2} is determined from the χ -T curves measured at various magnetic fields. A dramatic increase of H_{c2} with lowering temperature is clearly evidenced in the investigated temperature region.

The ac magnetic susceptibility measurements were adopted to make a further confirmation for the observed superconductivity. This technique has been successfully used to study numerous superconductors including high- T_c cuprates,⁴⁵ heavy-fermion material CeCu_2Si_2 ,⁴⁶ and iron-based FeSe_{1-x} .⁴⁷ The real component χ' of the ac susceptibility is a measure of the magnetic shielding, and the imaginary component χ'' reflects the magnetic irreversibility.⁴⁵ Figures 1(e) and 1(f) present the temperature dependence of χ'' and χ' of the ZFC ac susceptibility, respectively. For sample D (blue lines), two inflection anomalies occur in the χ'' -T and χ' -T curves upon cooling at the exact same temperature of 3.5 K, which coincides with the T_c value already determined from Fig. 1(a). As can be seen, both χ' and χ'' are close to zero above the transition due to the absence of flux exclusion in the normal state. Upon entering the SC state below 3.5 K, the diamagnetic behavior leads to a negative χ' which becomes more negative as more flux is expelled from the sample with lowering temperature. Here, a finite χ'' reflects the fact that the flux penetrating the sample lags the external flux. Similar inflection anomalies are also observed for sample E (red lines) around 3.5 K. However, only χ' exhibits an anomaly for the SC transition at 7.2 K and no visible change can be found for χ'' . This is attributed to the small fraction of the 7.2 K SC phase.

B. Crystal structures of pristine and potassium-doped triphenylbismuth

Figure 2 displays the XRD patterns of pristine and potassium-doped samples with $x = 1, 2,$ and 3 . The peak positions for the pristine material are in good agreement with the ones in the standard PDF card. Pristine triphenylbismuth is a typical kind of molecular solid and crystallizes in the space group $C2/c$ (No. 15), with eight molecules of $C_{18}H_{15}Bi$ in a unit cell of dimensions $a = 27.70 \text{ \AA}$, $b = 5.82 \text{ \AA}$, $c = 20.45 \text{ \AA}$, and $\beta = 114.48^\circ$,^{48,49} as shown in Fig. 3(a). The mean Bi-C distance is 2.24 \AA , and the mean C-Bi-C bond angle is about 94° . Upon doping potassium, no obvious peak appears at the positions where the pristine material shows strong peaks and the XRD feature is completely different from the undoped case. This indicates that doping of potassium atoms produces a new crystal structure.

Notice that the samples with different x 's exhibit a common XRD pattern marked by *, while the sample with $x = 2$ also shows a solitary pattern marked by #, which is actually consistent with the XRD pattern of metal Bi. The existence of Bi in sample E is evidenced by the appearance of colorless transparent liquid on the inner wall of the tube, indicating that partial triphenylbismuth molecules are decomposed into Bi atoms and phenyls. According to previous experimental and theoretical studies,^{50–54} the decomposed Bi might form K_3Bi with potassium at the annealing temperature of 130°C , while other K-Bi compounds such as KBi_2 , K_3Bi_2 ,

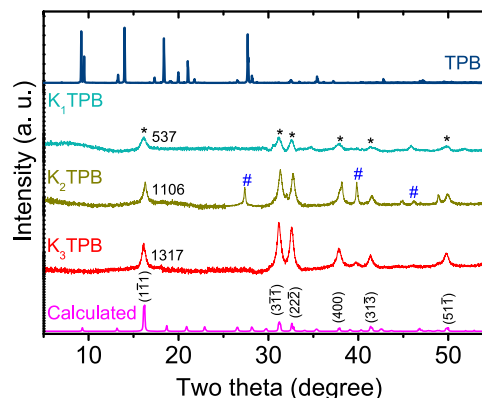


FIG. 2. XRD patterns of pristine and potassium-doped triphenylbismuth measured at room temperature. In Figs. 2 and 5, TPB, K_1TPB , K_2TPB , and K_3TPB correspond to pristine triphenylbismuth, samples B, E, and D, respectively. The symbol * represents the common XRD pattern for the three samples, and the symbol # stands for the solitary XRD pattern for sample E. The numbers beside the peak at 16.2° indicate the intensities of the first main peak of different samples. The purple curve at the bottom represents the calculated XRD pattern of an optimized structure in Fig. 3(b).

and K_5Bi_4 are hard to be produced since their formation temperatures are above 260°C , much higher than our annealing temperature. K_3Bi is a semimetal with the hexagonal $P6_3/mmc$ structure,^{52,55} and no superconductivity was reported for this compound. Therefore, superconductivity observed in our experiments is unlikely from the K-Bi compounds. Given that all the three samples exhibit superconductivity around 3.5 K ,

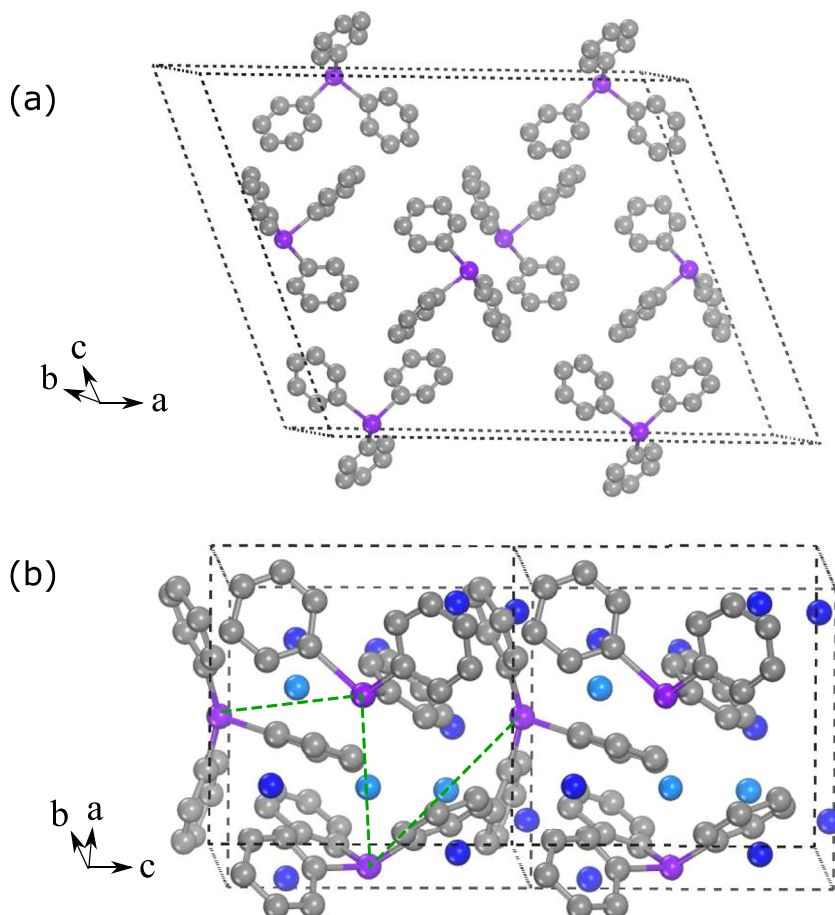


FIG. 3. (a) The molecular arrangement in pristine triphenylbismuth is shown in a single cell. (b) The arrangement of molecules and potassium in doped material is shown in a $2 \times 1 \times 1$ supercell. The grey, purple, and blue balls represent carbon, bismuth, and potassium atoms, respectively. The hydrogen atoms are not given in the figure for clarity.

it is reasonable to ascribe the 3.5 K SC phase to the crystal structure represented by *. It is interesting to see that the intensities of peaks marked by * increase according to the sample orders B, E, and D, accompanying with a rapid increase of SF from 0.01% to 3.74%. This positive correlation between structural and SC results, together with the evolution of the Raman intensities with the samples in Fig. 5, confirms that superconductivity actually comes from the crystal represented by *.

The grain sizes derived from the Debye-Scherrer equation according to the first XRD diffraction peak of potassium-doped samples are in the range from 11 to 18 nm, which is of the same order of magnitude as the typical London penetration depth. The comparability between the grain size and penetration depth makes the magnetic field pass through the sample grains even with a small applied field, leading to a dramatic reduction of the diamagnetic volume below T_c . This is the main reason for the small SFs listed in Table I. Another factor affecting the SF is decomposition of triphenylbismuth molecules, which reduces the proportion of K-doped triphenylbismuth in the synthesized materials. With increasing annealing time from one day to five days, it was found that more and more colorless transparent liquid appears on the inner wall of the tube, suggesting that an increasing number of triphenylbismuth molecules is decomposed into Bi atoms and phenyls. This experimental fact explains why the SFs are rather small for the samples annealed for five days. Meanwhile, the reduction of SF in the doped materials with more decomposed Bi safely excludes the possibility of K-Bi compounds induced superconductivity.

To identify the complicated crystal structure for the 3.5 K SC phase, we first make a search for global stable or metastable structures in the phase diagram of K_yBi with $y = 1-4$, which correspond to the possible arrangement of potassium and bismuth atoms in the doped materials. The searched results indicate that one cubic structure of K_4Bi could reflect the main character of the measured XRD pattern. Then we replace the bismuth atom with triphenylbismuth in this structure and perform a full relaxation of atomic positions. The optimized crystal has the PI space group, and the atomic positions of C, H, Bi, and K are given in the [supplementary material](#). In this crystal, three molecules of $C_{18}H_{15}Bi$ and twelve K atoms distribute in a nearly cubic unit cell of dimensions $a = 9.47 \text{ \AA}$, $b = 9.51 \text{ \AA}$, $c = 9.49 \text{ \AA}$, $\alpha = 89.62^\circ$, $\beta = 90.29^\circ$, and $\gamma = 89.85^\circ$, as shown in Fig. 3(b). Potassium atoms represented by blue balls in Fig. 3(b) are intercalated in the interstitial space of bismuth and phenyl rings, with the deep blue one close to a certain phenyl ring and the light blue one close to the center of the green dashed line connecting two bismuth atoms. The potassium concentration is estimated to be about $1.41 \times 10^{22}/\text{cm}^3$, slightly higher than the one in the potassium metal ($1.32 \times 10^{22}/\text{cm}^3$). The powder XRD pattern based on the optimized crystal, shown at the bottom of Fig. 2, is in good agreement with the one marked by *. This indicates that the doped materials crystallize into the optimized structure with high probability. The missing of weak peaks in K_xTPB ($x = 1-3$) compared with the theoretical modeling is mostly possible due to poor crystallization, manifested by broad XRD peaks in Fig. 2.

The orbital-resolved partial density of states (PDOS) for the optimized crystal is presented in Fig. 4. The existence of finite PDOS at the Fermi energy indicates that the potassium-doped system actually lies in the metallic state, providing a support for the observation of superconductivity at 3.5 K. Among the five orbitals shown in Fig. 4, the C-2p orbital makes a dominant contribution to PDOS in the vicinity of the Fermi energy, while the K-4s orbital has small contribution. This result reflects the fact that the electron is transferred from the K-4s to C-2p orbital, which not only leads to the metallic behavior but also strongly affects the vibrations of phenyl rings.

C. Raman spectra of pristine and potassium-doped triphenylbismuth

The SC phase was further characterized by phase-sensitive Raman spectroscopy. Five regions of Raman active modes from the low to high frequencies correspond to the lattice and Bi-phenyl, C-C-C bending, C-H bending, C-C stretching, and C-H stretching modes.⁵⁶ We observed all these modes in pristine triphenylbismuth. Upon doping potassium into triphenylbismuth, all lattice modes are dramatically suppressed and the modes in the C-H stretching region become invisible (see Fig. 5).

Significant differences of the spectra between the pristine and doped samples are in the C-H bending and C-C stretching regions. Upon doping potassium, the 644 and 993 cm^{-1} C-H bending modes in the pristine material shift down with a dramatic decrease in the intensity. By contrast, the C-H bending modes at 1154 and 1182 cm^{-1} shift up with an increase in the intensity. It is obvious that the mode intensity in the whole C-C stretching region gets a strong enhancement in the doped samples. An upshift of Raman spectra is also observed for the two peaks at 1322 and 1564 cm^{-1} in the pristine material, while the peak at 1469 cm^{-1} does not shift its position with the potassium doping.

The observation of both red and blue shifts of Raman spectra in potassium-doped triphenylbismuth is quite

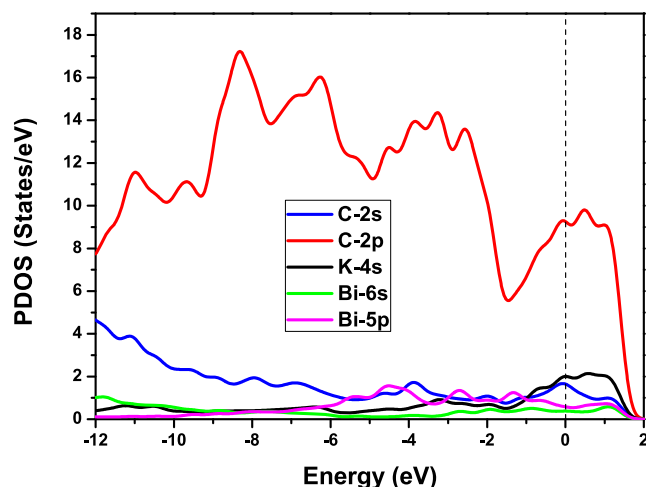


FIG. 4. Orbital-resolved partial density of states (PDOS) as a function of energy. The Fermi energy is set to be zero. The red, blue, black, green, and purple solid lines represent PDOS of C-2p, C-2s, K-4s, Bi-6s, and Bi-5p orbitals, respectively.

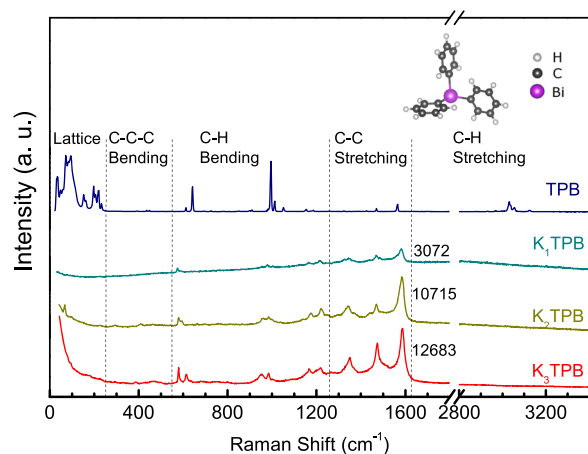


FIG. 5. Raman scattering spectra of pristine and potassium-doped triphenylbismuth collected at room temperature. The upper right figure presents the molecular structure of triphenylbismuth. Five regions of Raman active modes, divided by the vertical dashed lines, are shown above the spectra of the pristine material. The numbers beside the peak at 1584 cm^{-1} indicate the intensities of the strongest Raman peak of different samples.

different from the situation in potassium-doped phenanthrene¹⁴ and picene,²² where only red shifts were observed. Such red shifts were attributed to the softening of Raman modes by the transferred electrons from potassium to phenanthrene and picene molecules. This mechanism should also work for triphenylbismuth, making the Raman modes tend to shift down. On the other hand, when phenyl is connected to an X (either metal⁵⁷ or halogen⁵⁸) atom, both the C–H and C–C modes are affected by the C–X bond. In the halogeno-benzenes,⁵⁸ the frequencies of the C–C stretching modes increase from I-benzene to F-benzene, suggesting that an increase of benzene polarization with increasing electronegativity of halogen atoms makes the Raman modes tend to shift up. Based on the above analyses, the Raman shifts in our samples could be understood as the competing results between transferred electrons and enhanced polarization of phenyls, which is clearly manifested by the asymmetric Raman line shape and the increase of the Raman intensity in the C–C stretching region.

IV. CONCLUSIONS

The present results provide unambiguous evidence for highly reproducible superconductivity in potassium-doped triphenylbismuth. The existence of 3.5 K and 7.2 K SC transitions indicates that two stable crystal structures can be formed upon doping potassium into triphenylbismuth. The common 3.5 K SC phase is identified to have the triclinic P1 structure with a stoichiometry ratio of 4:1 between potassium and triphenylbismuth. Our theoretical calculations and measured Raman spectra reveal that superconductivity is produced by transferring electrons from potassium to carbon atoms on the phenyl rings. The findings of SC phases with much higher T_c 's (18 K in picene,¹³ 33 K in dibenzopentacene,¹⁵ and above 120 K in *p*-terphenyl^{16,17}) indicate that the arrangement of phenyl rings plays a crucial role in boosting superconductivity.

The unique feature of triphenylbismuth-like organometallic molecules is the presence of the metal atom connecting phenyl rings. Since the structure of such systems depends sensitively on the metal atom, finding materials with different T_c 's is expected, which provides a bottom-up understanding of the SC mechanism in the phenyl-ring-based organic superconductors.

SUPPLEMENTARY MATERIAL

See [supplementary material](#) for the CIF file of K-doped triphenylbismuth, which contains the atomic positions of C, H, Bi, and K in the unit cell.

ACKNOWLEDGMENTS

R.-S.W. and J.C. contribute equally to this work. We thank Hai-Qing Lin for strong support and valuable discussion. This work was supported by the National Natural Science Foundation of China under Grants Nos. 11574076, 11674087, and 91221103. Experiments in HPSTAR were supported by the National Key R&D Program of China (Grant No. 2018YFA0305900).

- ¹D. Jérôme, A. Mazaud, M. Ribault, and K. Bechgaard, *J. Phys. Lett.* **41**, 95–98 (1980).
- ²T. Ishiguro, K. Yamaji, and G. Saito, *Organic Superconductors*, 2nd ed. (Springer-Verlag, 1997).
- ³W. W. Li, E. Rose, M. V. Tran, R. Hubner, A. Lapinski, R. Swietlik, S. A. Torunova, E. I. Zhilyaeva, R. N. Lyubovskaya, and M. Dressel, *J. Chem. Phys.* **147**, 064503 (2017).
- ⁴A. F. Hebard, M. J. Rosseinsky, R. C. Haddon, D. W. Murphy, S. H. Glarum, T. T. M. Palstra, A. P. Ramirez, and A. R. Kortan, *Nature* **350**, 600–601 (1991).
- ⁵A. Y. Ganin, Y. Takabayashi, Y. Z. Khimyak, S. Margadonna, A. Tamai, M. J. Rosseinsky, and K. Prassides, *Nat. Mater.* **7**, 367–371 (2008).
- ⁶Y. Kasahara, Y. Takeuchi, R. H. Zadik, Y. Takabayashi, R. H. Colman, R. D. McDonald, M. J. Rosseinsky, K. Prassides, and Y. Iwasa, *Nat. Commun.* **8**, 14467 (2017).
- ⁷N. Emery, C. Hérold, M. d'Astuto, V. Garcia, Ch. Bellin, J. F. Mareche, P. Lagrange, and G. Loupias, *Phys. Rev. Lett.* **95**, 087003 (2005).
- ⁸J. S. Kim, L. Boeri, J. R. O'Brien, F. S. Razavi, and R. K. Kremer, *Phys. Rev. Lett.* **99**, 027001 (2007).
- ⁹K. Li, X. Feng, W. H. Zhang, Y. B. Ou, L. L. Chen, K. He, L. L. Wang, L. W. Guo, G. D. Liu, Q. K. Xue, and X. C. Ma, *Appl. Phys. Lett.* **103**, 062601 (2013).
- ¹⁰H. T. L. Nguyen, S. Nishiyama, M. Izumi, L. Zheng, X. Miao, Y. Sakai, H. Goto, N. Hirao, Y. Ohishi, T. Kagayama, K. Shimizu, and Y. Kubozono, *Carbon* **100**, 641 (2016).
- ¹¹Y. Cao, V. Fatemi, S. Fang, K. Watanabe, T. Taniguchi, E. Kaxiras, and P. Jarillo-Herrero, *Nature* **556**, 43–50 (2018).
- ¹²J. Miller, *Phys. Today* **71**(5), 15–19 (2018).
- ¹³R. Mitsuhashi, Y. Suzuki, Y. Yamanari, H. Mitamura, T. Kambe, N. Ikeda, H. Okamoto, A. Fujiwara, M. Yamaji, N. Kawasaki, Y. Maniwa, and Y. Kubozono, *Nature* **464**, 76–79 (2010).
- ¹⁴X. F. Wang, R. H. Liu, Z. Gui, Y. L. Xie, Y. J. Yan, J. J. Ying, X. G. Luo, and X. H. Chen, *Nat. Commun.* **2**, 507–513 (2011).
- ¹⁵M. Xue, T. Cao, D. Wang, Y. Wu, H. Yang, X. Dong, J. He, F. Li, and G. F. Chen, *Sci. Rep.* **2**, 389 (2012).
- ¹⁶R. S. Wang, Y. Gao, Z. B. Huang, and X. J. Chen, e-print [arXiv:1703.06641](#); e-print [arXiv:1703.05804](#); e-print [arXiv:1703.05803](#) (2017).
- ¹⁷W. Liu, H. Lin, R. Kang, X. Zhu, Y. Zhang, S. Zheng, and H. H. Wen, *Phys. Rev. B* **96**, 224501 (2017).
- ¹⁸P. Neha, A. Bhardwaj, V. Sahu, and S. Patnaik, *Physica C* **554**, 1–7 (2018).
- ¹⁹H. Li, X. Zhou, S. Parham, T. Nummy, J. Griffith, K. Gordon, E. L. Chronister, and D. S. Dessau, e-print [arXiv:1704.04230](#) (2017).
- ²⁰P. L. de Andres, A. Guijarro, and J. A. Verges, *Phys. Rev. B* **83**, 245113 (2011).

- ²¹T. Kosugi, T. Miyake, S. Ishibashi, R. Arita, and H. Aoki, *Phys. Rev. B* **84**, 214506 (2011).
- ²²T. Kambe, X. He, Y. Takahashi, Y. Yamanari, K. Teranishi, H. Mitamura, S. Shibusaki, K. Tomita, R. Eguchi, H. Goto, Y. Takabayashi, T. Kato, A. Fujiwara, T. Kariyado, H. Aoki, and Y. Kubozono, *Phys. Rev. B* **86**, 214507 (2012).
- ²³B. Mahns, F. Roth, and M. Knupfer, *J. Chem. Phys.* **136**, 134503 (2012).
- ²⁴A. Ruff, M. Sing, R. Claessen, H. Lee, M. Tomić, H. O. Jeschke, and R. Valentí, *Phys. Rev. Lett.* **110**, 216403 (2013).
- ²⁵X. W. Yan, Z. B. Huang, and H. Q. Lin, *J. Chem. Phys.* **139**, 204709 (2013).
- ²⁶Q. W. Huang, G. H. Zhong, J. Zhang, X. M. Zhao, C. Zhang, H. Q. Lin, and X. J. Chen, *J. Chem. Phys.* **140**, 114301 (2014).
- ²⁷X. W. Yan, Z. B. Huang, and H. Q. Lin, *J. Chem. Phys.* **141**, 224501 (2014).
- ²⁸S. Shahab Naghavi and E. Tosatti, *Phys. Rev. B* **90**, 075143 (2014).
- ²⁹G. A. Artioli, F. Hammerath, M. C. Mozzati, P. Carretta, F. Corana, B. Mannucci, S. Margadonna, and L. Malavasi, *Chem. Commun.* **51**, 1092 (2015).
- ³⁰S. Heguri, M. Kobayashi, and K. Tanigaki, *Phys. Rev. B* **92**, 014502 (2015).
- ³¹Y. Kubozono, R. Eguchi, H. Goto, S. Hamao, T. Kambe, T. Terao, S. Nishiyama, L. Zheng, X. Miao, and H. Okamoto, *J. Phys.: Condens. Matter* **28**, 334001 (2016).
- ³²X. F. Wu, C. Q. Xu, K. D. Wang, and X. D. Xiao, *J. Phys. Chem. C* **120**, 15446 (2016).
- ³³Y. Gao, R. S. Wang, X. L. Wu, J. Cheng, T. G. Deng, X. W. Yan, and Z. B. Huang, *Acta Phys. Sin.* **65**, 077402 (2016).
- ³⁴X. W. Yan, Y. Y. Wang, M. Gao, D. W. Ma, and Z. B. Huang, *J. Phys. Chem. C* **120**, 22565 (2016).
- ³⁵F. D. Romero, M. J. Pitcher, C. I. Hiley, G. F. S. Whitehead, S. Kar, A. Y. Ganin, D. Antypov, C. Collins, M. S. Dyer, G. Klupp, R. H. Colman, K. Prassides, and M. J. Rosseinsky, *Nat. Chem.* **9**, 644–652 (2017).
- ³⁶Y. Takabayashi, M. Menelaou, H. Tamura, N. Takemori, T. Koretsune, A. Stefancic, G. Klupp, A. J. C. Buurma, Y. Nomura, R. Arita, D. Arcon, M. J. Rosseinsky, and K. Prassides, *Nat. Chem.* **9**, 635–643 (2017).
- ³⁷G. H. Zhong, X. H. Wang, R. S. Wang, J. X. Han, C. Zhang, X. J. Chen, and H. Q. Lin, *J. Phys. Chem. C* **122**, 3801 (2018).
- ³⁸C. Elschenbroich, *Organometallics*, 3rd ed. (Wiley-VCH-Verlag, Weinheim, 2006).
- ³⁹M. Dötterl and H. G. Alt, *ChemCatChem* **4**, 370–378 (2012).
- ⁴⁰C. W. Glass, A. R. Oganov, and N. Hansen, *Comput. Phys. Commun.* **175**, 713–720 (2006).
- ⁴¹G. Kresse and J. Hafner, *Phys. Rev. B* **47**, 558–561 (1993).
- ⁴²G. Kresse and J. Furthmüller, *Phys. Rev. B* **54**, 11169–11186 (1996).
- ⁴³J. P. Perdew, K. Burke, and M. Ernzerhof, *Phys. Rev. Lett.* **77**, 3865–3868 (1996).
- ⁴⁴P. E. Blöchl, *Phys. Rev. B* **50**, 17953–17979 (1994).
- ⁴⁵F. Gömöry, *Supercond. Sci. Technol.* **10**, 523–542 (1997).
- ⁴⁶E. Lengyel, M. Nicklas, H. S. Jeevan, C. Geibel, and F. Steglich, *Phys. Rev. Lett.* **107**, 057001 (2011).
- ⁴⁷M. Bendele, A. Amato, K. Conder, M. Elender, H. Keller, H.-H. Klaus, H. Luetkens, E. Pomjakushina, A. Raselli, and R. Khasanov, *Phys. Rev. Lett.* **104**, 087003 (2010).
- ⁴⁸D. M. Hawley and G. Ferguson, *J. Chem. Soc. A* **1968**, 2059–2063.
- ⁴⁹P. G. Jones, A. Blaschette, D. Henschel, and A. Weitze, *Z. Kristallogr.* **210**, 377–378 (1995).
- ⁵⁰G. Gnutzmann and W. Klemm, *Z. Anorg. Allg. Chem.* **309**, 181–188 (1961).
- ⁵¹A. Petric, A. D. Pelton, and M. L. Saboung, *J. Phys. F: Met. Phys.* **18**, 1473–1489 (1988).
- ⁵²A. Petric and A. D. Pelton, *J. Phase Equilib.* **12**, 29–33 (1991).
- ⁵³K. Hochgesand and R. Winter, *J. Chem. Phys.* **112**, 7551–7556 (2000).
- ⁵⁴C. Niu, C. Li, Z. Du, C. Guo, and M. Liu, *Thermochim. Acta* **528**, 9–14 (2012).
- ⁵⁵J. Wen, H. Guo, C. H. Yan, Z. Y. Wang, K. Chang, P. Deng, T. Zhang, Z. D. Zhang, S. H. Ji, L. L. Wang, K. He, X. C. Ma, X. Chen, and Q. K. Xue, *Appl. Surf. Sci.* **327**, 213–217 (2015).
- ⁵⁶C. Ludwig and H.-J. Götze, *Spectrochim. Acta, Part A* **51**, 2019–2026 (1995).
- ⁵⁷K. Shobatake, C. Postmus, J. R. Ferraro, and K. Nakamoto, *Appl. Spectrosc.* **23**, 12–16 (1969).
- ⁵⁸D. H. Whiffen, *J. Chem. Soc.* **1956**, 1350–1356.